Nanoscale Abrasive Wear of Polyethylene: A Novel Approach To Probe Nanoplastic Release 1 at the Single Asperity Level 2 [‡]Ehsanur Rahman¹, [‡]Sara BinAhmed¹, Phoebe Keyes¹, Claire Alberg¹, Stacy Godfreey-Igwe², 3 Greg Haugstad³, *Boya Xiong¹ 4 5 6 1. Department of Civil, Environmental, and Geo-Engineering, University of Minnesota, 500 Pillsbury Dr SE, Minneapolis, Minnesota 55455, United States 7 2. Department of Mechanical Engineering, Massachusetts Institute of Technology, 33 8 9 Massachusetts Ave, Cambridge, Massachusetts 02139, United States 3. Characterization Facility, University of Minnesota, 100 Union St. SE, Minneapolis, Minnesota 10 11 55455, United States 12 [‡]Both authors contributed equally to this work. 13 *Corresponding author: bxiong@umn.edu; Tel.: +1 8149542509 14 15

Word count: Abstract, and main manuscript (5521) + Figure 1 (300) + Figure 2 (300) + Figure 3

(300) + Figure 4 (300) + Figure 5 (300) + Figure 6 (300) = total 7321

16

17

Abstract:

19

There is a growing concern that nanoplastic pollution may pose planetary threats to human and 20 ecosystem health. However, a quantitative and mechanistic understanding of nanoplastic release 21 22 via nanoscale mechanical degradation of bulk plastics and its interplay with photoweathering remains elusive. We developed a lateral force microscope (LFM) based nanoscratch method to 23 investigate mechanisms of nanoscale abrasive wear of low-density polyethylene (LDPE) surfaces 24 25 by a single sand particle (simulated by a 300 nm tip), under environmentally relevant load, sliding motion, and sand size. For virgin LDPE, we found plowing as the dominant wear mechanism (i.e., 26 deformed material pushed around the perimeter of scratch). After UVA-weathering, the wear 27 mechanism of LDPE distinctively shifted to cutting wear (i.e., deformed material detached and 28 29 pushed to the end of scratch). The shift in the mechanism was quantitatively described by a new parameter, which can be incorporated into calculating the NP release rate. We determined a 10-30 fold higher wear rate due to UV weathering. We also observed an unexpected resistance to initiate 31 wear for UV-aged LDPE, likely due to nanohardness increase induced by UV. For the first time, 32 we report $0.4-4\times10^{-3}$ µm³/µm sliding distance/µN applied load as an initial approximate 33 nanoplastic release rate for LDPE. Our novel findings reveal nanoplastic release mechanisms in 34 35 the environment, enabling physics-based prediction of the global environmental inventory of nanoplastics. 36

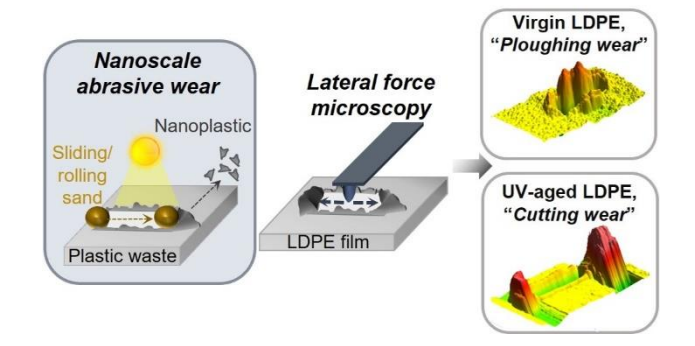
37 **Keywords:**

- 38 nanoplastics, mechanical degradation of polymer, lateral force microscopy, nanoscale wear,
- 39 photooxidation, fragmentation, nanotribology.

40 Synopsis:

- This study reveals fundamental insights into nanoscale abrasive wear of polyethylene and the
- 42 impact of UV-weathering with implications for nanoplastic release.

44 Graphic Abstract



47 Introduction

Plastic breakdown products, micro- and nanoplastics (MPs and NPs)^{1, 2} pose urgent threats to human health,³⁻⁵ ecosystem functions,⁶⁻⁹ and global climate.¹⁰⁻¹² NPs (size < 1 μm) are potentially more harmful than MPs, because of their higher extent of environmental transport and exposure to organisms and size-dependent toxicity effects.¹³⁻¹⁵ NPs are generated from photodegradation,^{16, 17} mechanical fragmentation/abrasion,¹⁸⁻²¹ and thermal degradation²¹⁻²³ of bulk plastics. Specifically, mechanical degradation is recognized as a critical mechanism in many scenarios^{20, 24-26}; however, it remains poorly quantitatively and mechanistically understood. Unlike photodegradation in which UV-dose translates data from the laboratory to the field,²⁷ current mechanical degradation methods (e.g., the rotational speed of a shaker^{28, 29}) cannot quantify the input energy or force¹⁶. A few studies attempted to quantify the input energy deployed mN-kN range load, generating primarily MPs.^{18, 26, 30} Mechanical processes that specifically release NPs remain unexplored.

In addition to sequential *bulk* fragmentation of photodegraded plastics,³¹⁻³³ a growing literature has highlighted the role of *surface* degradation for MP/NP release.^{16, 34} Surface mechanical degradation of plastics can be described as various modes of wear (adhesive, abrasive, and fatigue^{35, 36}), resulting from the relative motion between two contacting surfaces. In particular, abrasive wear³⁷ is the deformation of *soft* material caused by collision or sliding of *hard* solid and/or protruding features (e.g., roughness³⁸). Frequently, soft plastics co-occur with hard inorganic particles (their hardness differs by 1-2 decades^{39, 40}), during their cotransport in wind and soil erosion,⁴¹ storm runoff,²⁴ and beaches.²⁸ Thus, compared to other wear mechanisms, we hypothesize that abrasive wear is one of the dominant mechanisms that directly generates NPs in the environment.

Previous abrasive wear studies are mostly at the micro- and macroscale, utilizing abrasive papers, ^{26, 30} pin-on-disk device, ^{42, 43} and abrasive slurry, ⁴⁴ generating micrometer scale wear debris. Limited studies have investigated the mechanisms and rates of *nanoscale* abrasive wear that predominantly releases NPs. Atomic force microscopy (AFM), in particular, lateral force microscopy (LFM) is ideal for mechanistically exploring nanoscale abrasive wear, ^{45, 46} as the AFM tip can simulate a single asperity contact with a solid surface. LFM utilizes a scan perpendicular to the cantilever axis, resulting in friction-actuated cantilever torsion, which can be captured as a

lateral deflection to yield absolute friction force.⁴⁷ Thus, LFM offers nanoscale spatial resolution of friction and topography under a controlled normal load. This approach has enabled the mapping of nanoscale wear of inorganic⁴⁸⁻⁵⁰ or carbonaceous materials⁵¹ but has not been widely utilized for detailed wear mechanism and rates analysis for polymers, particularly polyolefins.⁵² Furthermore, such an approach has not been used for studying photooxidized polymers. For semicrystalline polyolefins, photooxidation is known to cause substantial MW reduction, oxidation, chemicrystallization, and loss of bulk ductility.⁵³ Very limited studies examined the effect of UV⁵⁴ or gamma irradiation⁵⁵ on microscale wear. However, the effect of photooxidation on surface nanomechanical properties and nanoscale abrasive wear behavior remains unknown.

Here, we developed a novel LFM-based nanoscratch test, followed by imaging, to explore the fundamental mechanisms and rates of nanoscale abrasive wear of low-density polyethylene (LDPE) and the impact of photoweathering. Through nanoscale control and measurement of forces and topography, our method enables us to: (1) apply forces that are relevant in natural sediment transport, (2) elucidate the onset and mechanisms of nanoscale abrasive wear at the single-asperity level, and (3) quantity wear rate per unit force as an approximate nanoplastic release by sand abrasion via sliding motion. To the best of our knowledge, this is the first time such a method has been applied to polymer materials to inform nanoplastic release mechanisms in the environment and to demonstrate the contrasting wear behavior of LDPE at the nanoscale before and after UV-weathering.

Materials and Methods

Material and Photooxidation of LDPE

A commercial LDPE homopolymer film (101.6 μm thick, BFI345-013, Blueridge Films Inc., VA, USA) was studied as a model polyolefin. After DI water rinsing and overnight drying, the LDPE films were weathered using a QUV/SE (Q-Lab, Ohio, USA) at 1.55 W/m² (340 nm) and 60°C for 50 days without condensation (ASTM G154). No temperature or humidity was changed during the UV aging of LDPE. Facile breakage of the film when transferred by tweezers suggested that the UV exposure resulted in complete LDPE embrittlement. A ~1 cm × 1.5 cm LDPE piece was glued to a glass slide using epoxy for all AFM experiments.

Friction Measurements

LFM was used to explore the sliding friction characteristics between the LDPE samples and silica under dry conditions by using an MFP3D-Bio Atomic Force Microscope (Asylum Research, Santa Barbara, CA). A rounded silicon probe (SD-R150-FM-10, NanoAndMore USA Corp, Santa Clara, CA) with a radius of 150 nm and a spring constant of 3.5 N/m was used. The size and chemistry of the probe were selected to represent fine sediments or sand surface nanoroughness. Although natural sand and soil grains range from 0.1 to 10 mm in diameter, their surface roughness at both vertical and lateral scales has been determined to be sub-μm to a few μm using optical interferometry. S8, S6, S8, S9 Such a range of roughness has also been deployed for studying roughness effects on porous media asperities and pore-scale transport. The normal spring constants of all probes used in this study were calibrated using the thermal noise method in conjunction with collecting force-Z curves on freshly cleaved mica to determine the optical lever sensitivity.

To measure friction and loading force, lateral deflection and the z-sensor were simultaneously collected at constant vertical cantilever deflection (i.e., measured normal load). Friction force was quantified as the difference of the lateral signals of trace (sliding in one direction) and retrace (sliding in the opposite direction) with a sign included (i.e., friction loop)⁴⁷ using Gwyddion (version 2.59). For friction force maps (x and y scan enabled), the wearless frictional regime was probed under 50 nN, 128 points/loop, and 128 loops in total at a rate of 0.25 Hz. For friction measurements as a function of load, a built-in software function was used to automate load ramping at each friction loop for 64 loops from zero until the maximum set load was reached. The raw lateral signals in V to absolute friction force in nN was converted using eq 1 with the LFM measurements using the same silica probe on mica and the known coefficient of friction between mica and silicon (0.168⁶⁰):

129
$$f = \frac{(lateral\ trace\ signal\ -\ lateral\ retrace\ signal)}{2} \times \frac{\mu_{mica}}{m}$$
 (1)

where, f is the friction, m is the slope of raw lateral signals in V versus normal load on a clean mica, and μ_{mica} is the coefficient of friction of silicon on mica (Figure S1 and Table. S1). Proper tip cleaning and quality control were performed to ensure the consistency of tip status between different friction experiments (Figure S2). Both friction experiments were repeated on 5 different spots on the same coupon for each sample.

Nanoscratch Abrasion Experiments

A nanoscratch test was developed to perform the single asperity abrasive wear of LDPE at the nanoscale, followed by topography imaging (details in the SI). A rounded silicon tip (SD-R150-NCL-10, NanoAndMore, USA Corp, CA) with a radius of 150 nm and a spring constant of 42 N/m was used. Under one normal load ($2-6 \mu N$), nanoscratch was performed in one dimension for 1.5 μm with slow scan disabled, back and forth repetitively for 10 times, at a sliding speed of 374.64 nm/s. The justification for selecting the range of load is detailed in the Results and discussion. One tip was used for one set of nanoscratch tests, which included triplicate scratches under one load for five loads in total, consecutively. Following the nanoscratch experiment, we switched to a sharp tip (AC240TS-R3, radius of 7 nm, 70 Hz, 2 N/m, Oxford Instruments Company) to image the scratched area in AC/tapping mode ($4\times4 \mu m^2$ for 512 lines and 512 points/line). The topography images were analyzed using Gwyddion to calculate the volume of the scratched area (details in the SI). For each sample, one set of nanoscratch tests was repeated on 3-5 different pieces of coupons (n=8-13 under each load).

Nanoindentation Experiments

Elastic modulus and hardness of LDPE films were obtained by nanoindentation experiments using AFM. 61-63 Compared to the widely used tensile tests that interrogate bulk properties, 64-66 nanoindentation can provide surface nanomechanical properties, which are more relevant to the nanoscale surface wear. A spherical SiO probe (CP-FM-SiO-A, NANOSENSORS, Switzerland) with a spring constant of 2.8 N/m and a radius of 1000 nm was used (Figure S3). For each LDPE sample, 30 force curves were collected on random locations of 2 different coupons. The force curves were fitted to the appropriate contact mechanics model based on the transition parameter using a customized MatLab code to calculate the elastic modulus and hardness of LDPE samples (SI).

Surface Chemistry, Molecular, Structural, and Morphological Characterization of LDPE

The experimental details of characterization and analysis of the carbonyl index (CI= $\frac{I_{1715}}{I_{1472}}$), ⁶⁷ contact angle, molecular weight, surface roughness, bulk crystallinity, and photothermal AFM-IR of the pristine and UV-aged LDPE are included in SI using well-established methods.

Results and Discussion

Photooxidation Leads to Oxidation, Chain scission, and Chemicrystallization.

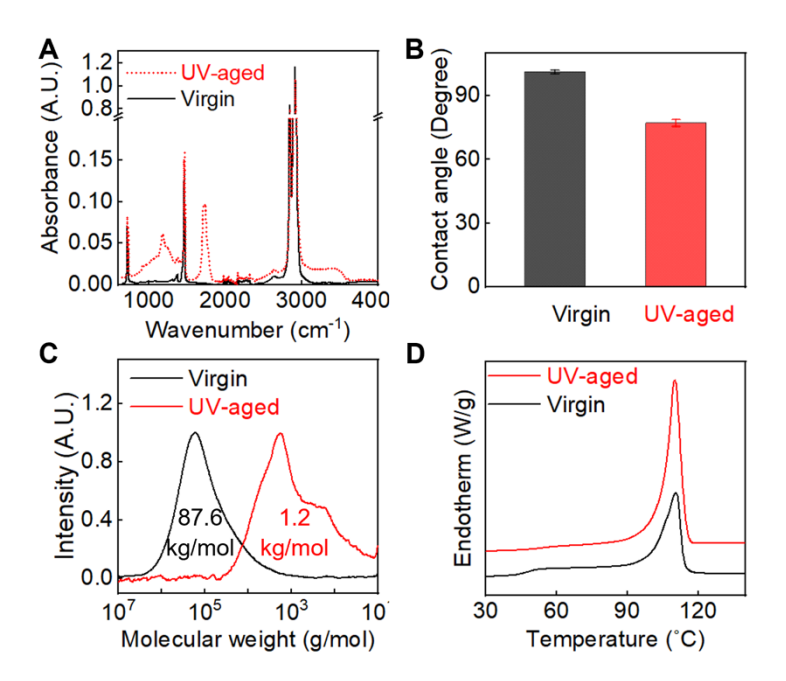


Figure 1. Photoweathering under UVA at 60 °C led to oxidation, chain scission, and chemicrystallization of LDPE. (**A**) IR spectra showed a 63-fold increase in carbonyl index (1713 cm⁻¹). (**B**) Decreased contact angle suggested an increase in hydrophilicity. (**C**) GPC traces showed a near 100-fold reduction in weight average MW. (**D**) DSC thermogram showed a 2-fold increase in χ_c (23–43%). LDPE with a thickness of 101.6 μ m was UV-aged in air for 50 days using a modified ASTM G154 method without condensation (1.55 W/m², 340 nm, 60 °C).

A combination of characterization techniques evidenced substantial chain scission, oxidation, and chemicrystallization because of the photo-oxidation of LDPE (Figure 1). ATR-FTIR (Figures 1A and S4A,B) results suggested a substantial increase in carbonyl groups (1650–1850 cm⁻¹) for LDPE after photooxidation, with the carbonyl index (CI) increased from 0.011 to 0.694 (peak area increased from 0.19 to 8.2 in 1650–1850 cm⁻¹), consistent with many previous observations.⁶⁸⁻⁷⁰ The carbonyl group can be deconvolved into ketones or carboxylic acids (1710–1713 cm⁻¹) and esters and/or aldehydes (1734 cm⁻¹) as products of photooxidation. Furthermore, AFM-IR imaging analysis showed that the carbonyl peak intensity (1713 cm⁻¹) was minimal across the thickness of the virgin LDPE (Figures S5 and S6); in comparison, a clear carbonyl peak appeared homogeneously over the entire 100 μm thickness of the UV-aged LDPE. These results further demonstrate that our UV-aged LDPE was homogeneously oxidized across

the thickness and completely embrittled. The IR-detected oxidation was consistent with increased hydrophilicity measured as a decline from 101.3 ± 0.8 to 77.2 ± 1.6 in the contact angle of LDPE after photooxidation (Figure 1B). A similar reduction in contact angle after UV exposure was observed.^{24, 71-73} In addition, chain scission was observed up to nearly two orders after photooxidation according to high-temperature GPC (from 87.6 to 1.2 kg/mol) (Figure 1C). Finally, we observed a 2-fold increase in the degree of crystallinity (23.3 \pm 0.3 to 43.1 \pm 1.4%) after photooxidation by DSC analysis (Figures 1D and S4C), measured as the enthalpy of fusion at the melting temperature of the sample relative to that of a perfect crystal (293.6 J/g⁷⁴). Such an increase in crystallinity due to photooxidation has been referred to as chemi-crystallization,⁷⁴ in which the broken chains have sufficient mobility to recrystallize along the existing lamellar structures. In addition, we observed facile breakage of the film, while it was being transferred using a tweezer. This is qualitative evidence that the ductile LDPE has been embrittled so that the strain at break is likely near zero.

Photooxidation Increases wearless Sliding Friction and Delays the Onset of Wear of LDPE.

Wearless Sliding Friction

Wearless frictional contact is the first solid-solid interaction prior to wear, which also contributes to abrasive wear. The wearless frictional regime is the linear regime of friction force (f) versus the normal load (F). For virgin LDPE, we observed such linearity ($R^2 > 0.98$) with normal load up to 335.16 ± 103.32 nN (n=5, Figures 2A, S7 and Table S2) and f<17 nN. The kinetic friction coefficient, $\mu = \frac{f}{F}$, was calculated to be 0.031 ± 0.004 (n=5). Similar friction coefficients were found for PE (0.06)⁷⁵ and HDPE (0.1)⁷⁶ using comparable tip size and normal load. In comparison, photooxidized LDPE had a μ value of 0.066 ± 0.002 (Figures 2A, S8 and Table S2), 2-fold higher than that of virgin LDPE (paired t-test, p = <0.05) and an overall higher f (< ~50 nN). Spatial mapping of wearless f (Figure 2B=D) revealed that the average f of LDPE was 1.72-fold higher after photoweathering (42.78 ± 10.18 nN compared to 24.77 ± 4.89 nN, p = 0 < 0.05). Furthermore, the higher variance of f suggested a more heterogeneous surface in terms of friction after photoweathering. We note that spatial friction force was not associated with topographical details (Figure S9).

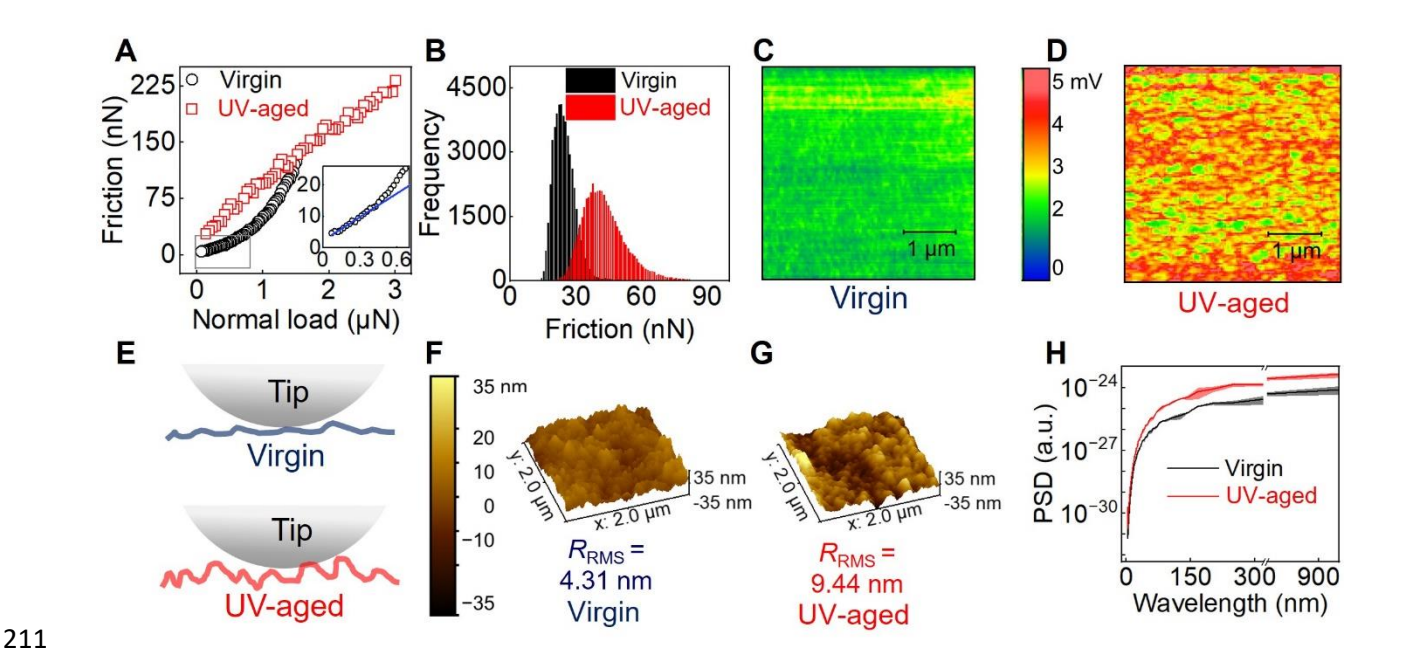


Figure 2. (A) Friction vs normal load curve for virgin and photooxidized LDPE. Inset: A representative of friction-to-wear transition (onset of wear) for virgin LDPE. (B) Histograms of friction under 50 nN load over a 4×4 µm area, $n=3\times49,152$ data points for 3 different locations on each sample. The friction of virgin LDPE ranged from 0.11 to 57.02 nN with a variance of 23.87 nN, in comparison to 5.38–113.45 nN for UV-aged LDPE (variance of 103.54 nN). A representative friction image of (C) virgin LDPE and (D) UV-aged LDPE (data shown in B). (E) Illustration of the multiasperity contact between tip and LDPE surface, where UV-aged LDPE had a higher roughness at all lateral scales. Topography images of (F) virgin LDPE and (G) UV-aged LDPE and the calculated root-mean-square roughness (R_{RMS}). (H) Linear power spectral density function plotted with wavelength (inverse of spatial frequencies multiplied by 2π) demonstrated a higher frequency of lateral roughness features for UV-aged LDPE compared with virgin LDPE.

The friction of polymers can result from (1) internal viscoelastic dissipation⁷⁷ from tip-polymer interaction affected by crystallinity⁷⁸ and glass transition temperature (T_g) ,⁷⁹ (2) noncovalent surface chemical interactions,⁸⁰ and (3) surface roughness relative to the size of the counterface.^{81, 82} First, a more crystalline LDPE would have reduced energy dissipation and friction force,⁸³ opposite to what we observed. Similarly, a previous outdoor weathering study on HDPE revealed an increase in T_g and a decrease in free volume,⁸⁴ which would have also led to lower friction. Second, the enhanced polarity and hydrophilicity of the oxidized LDPE surface (Figure 1 A, B) will induce a stronger dipole-dipole interaction between the tip and sample, leading to higher friction force.⁷² Third, surface roughness of UV-aged LDPE was higher (Figure 2E): R_{RMS} increased from 4.31 \pm 0.33 to 9.44 \pm 1.12 nm (Figures 2F, G and S10), consistent with previous findings.^{66, 73} Furthermore, the lateral feature analyzed by the power spectral density

function (PSDF) (Figure 2H) and topography images (Figures S11 and S12) suggested that a significant fraction of the lateral features of both samples was lower than the size of the AFM tip (Figure 2 E). Therefore, the measured friction resulted from multiasperity contacts between the tip and samples. From the PSDF plots, the amplitude at all wavelengths was higher for the UV-aged LDPE, further suggesting that UV exposure increased the roughness of the entire size range of the lateral features. Our detailed analyses revealed that a higher nanoscale wearless sliding friction of LDPE after photoweathering was mainly derived from surface chemistry/energy and roughness-dependent multiasperity interactions.

The Onset of Wear

234

235

236

237

238

239

240

241

242

243

244

245

246

247

248

249

250

251

252

253

254

255

256

257

258

259

260

261

When increasing the load to near the wear point (onset of wear), the lateral signal will have an additional contribution from material deformation (wear), leading to a distinct change in the slope of a friction force versus load curve⁴⁷ (Figure 2 A, inset). Measuring the onset of wear could inform the critical load and energy input to trigger NPs generation from the nanoscale abrasive wear of LDPE. For virgin LDPE, the wear point was around 335.16 ± 103.32 nN (n=5, Figure S5 and Table S2). Surprisingly, we observed no clear change of the slope for UV-aged LDPE up to 3 μN load (n=5, Figure S6 and Table S2), suggesting an over 1 order of magnitude suppression of the onset of wear, derived from photoweathering. The result indicates that it requires more input of force and energy to initiate NPs release via the nanoscale abrasive wear mechanism for UVaged LDPE. This is counterintuitive to the prevailing understanding that photooxidized PE, PP, PS, PET, thermoplastic polyurethane, and polyamide are more likely to release MP/ NPs. ^{28, 85,69}, ⁸⁶ Details of the underlying mechanisms are discussed next. The gravitational force of one single sand grain with typical diameters that can undergo creep motion^{87, 88} in the air can provide 2 nN to 13 μN force (SI). Therefore, our finding on the onset of wear suggests that there could be a critical sand grain size that leads to the onset of abrasion of LDPE, which is UV-aging dependent. We note that photoweathering alone can directly lead to NP release in aqueous environments, through other release mechanisms (in the presence of water 16, 86 surfactants 19, and fluid shear stress). This is the first report that UV-aged LDPE can delay the onset of wear at the nanoscale.

Novel Nanoscratch Test Reveals Transition of Nanoscale Wear Mechanism during

262 Photoweathering.

Our AFM-based nanoscale abrasive wear tests using μN range forces and a 300 nm diameter silicon tip were performed on LDPE to simulate abrasion by rolling and sliding sand (Figure 3A). This range of load can represent the estimated gravitational force of one single sand grain described above^{87, 88}(SI). More importantly, our nanoscratch tests can detail the wear mechanism at the single asperity level, which was not possible with other degradation and wear methods.

For virgin LDPE, abrasive wear under $F = 2-6 \mu N$ created scratch topographies (i.e., grooves) with a depth ranging from 50 to 300 nm and a width ranging from 100 to 500 nm (Figures S13 and S14). The abraded materials were pushed outside of the scratch and piled up around the periphery of the scratch (Figure 3 B, D). These pile-up materials had nanometer to sub- μ m features, with a height of \sim 50–300 nm and a width of \sim 100–500 nm, which can be NPs if released. These features were typically long and thin, with some areas being "wavy" and partially covering the apparent scratch area. In addition, polymer transfer onto tips was observed after nanoscratch experiments (Figure 3 E, G), indicating co-occurring adhesive wear^{35, 36, 89} (deformation by sliding of two surfaces with similar hardness). Such adhered polymer can be released as NPs via subsequent sand collision, or cotransport with sand.

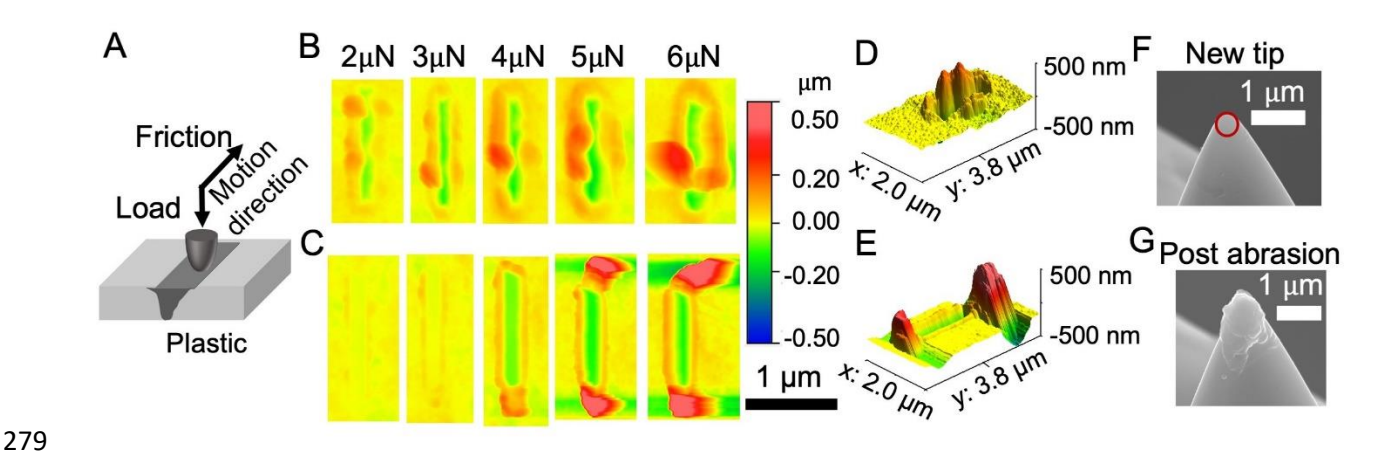


Figure 3. **(A)** Illustration of the single asperity nanoscratch test using LFM. Nanoscale wear topography with increasing load for **(B)** virgin and **(C)** UV-aged LDPE suggested a clear wear mechanism transition from plowing/wedge formation to cutting wear due to photoweathering and load. The three-dimensional (3D) image of the abraded area of **(D)** virgin and **(E)** UV-aged LDPE under 4 μ N. The pile-up refers to the orange to red area accumulated around the scratch, and the scratch refers to the yellow to green color inside the groove or the scratch itself. We note that the presented scratch topography was obtained after 10 repeated sliding events. SEM image of 150

nm radius rounded silicon tip (**F**) before and (**G**) post nanoscratch experiment, suggesting transfer of polymer to tip. The postabrasion SEM image of the tip was taken after being used for creating 15 scratches (i.e., 3 repeated scratches under each load from 2 to 6 μ N).

In comparison, UV-aged LDPE had a lower scratch depth from near zero to 150 nm and a similar width as virgin LDPE (Figure S14). At load > 4 μ N, distinctively, the abraded materials were pushed and accumulated at the scratch ends, with little material remaining along the side of the scratch (Figure 3 C, E). The pile-up features at scratch ends were fragment and sphere-like (compared to ribbon or flake-like observed in virgin polymer⁷⁸ and steel⁹⁰) and had a width of up to 1 μ m and a height of up to 500 nm. Releasing the entire pile-up at the scratch end would lead to the formation of a near μ m-range NPs particle.

Kato and co-workers. 90-92 defined three wear mechanisms for microscale abrasive wear of metals based on in situ scanning electron microscopy observation. Plowing refers to groove formation and deformed material accumulation along the scratch. Cutting refers to wear debris being pushed to the scratch end continuously during sliding. Wedge formation is between plowing and cutting, where only the initially formed wear debris during sliding can accumulate at the scratch end. Our scratch topography of virgin LDPE clearly suggested a plowing and wedge formation mechanism, 90 which was transitioned to primarily cutting wear for the UV-aged LDPE at 4–6 µN. The observed differences in wear mechanism between virgin and UV-aged LDPE are likely related to the difference between the wear of a ductile and brittle material, generally observed for metals and polymer composites. 91,93,94 Furthermore, at 2–3 μ N, the wear mechanism of UV-aged LDPE remained at plowing and wedge formation, suggesting that the wear mechanism changed as a function of load, more so for UV-aged LDPE than virgin ones (Figure 3C). This loaddependent wear mechanism transition was previously discovered by Kato⁹¹ for microscale wear of metals and steels (plowing-wedge formation-cutting). This is the first time that the wear mechanism transition of LDPE was revealed after UV exposure. Such distinct wear mechanisms can imply a change in the wear rate, in other words, NPs release rate (next section).

Other wear modes including fatigue wear and crack formation generating micrometer to millimeter scale debris have been widely observed for polymer materials by micro- and macroscale wear studies.^{24, 26, 43, 95} Notably, we did not observe such types of wear for virgin LDPE in our study. Surprisingly, cracking was not observed for the completely embrittled UV-aged LDPE. This might be due to the presence of additives (e.g., antioxidants), which require further investigation.

Our results clearly suggested a distinct wear mechanism at the nanoscale (plowing/cutting) and in the investigated force range compared to the findings from macroscale studies (fatigue/cracking).

The First Estimation of the Nanoscale Abrasive Wear Rate of LDPE at the Single Asperity Level.

NPs are released from abrasion when the deformed material is either transferred onto the abrasive particle (Figure 3F, G) or detached from the original surface. The three mechanisms of wear described above were originally categorized by Kato *et al.*90-92 based on their likelihood of loose wear debris release. In cutting wear, pile-up materials are physically moved to the scratch end, strongly implying the complete detachment of the pile-up from the original surface. Specifically, Kayaba *et al.*90 observed that the cutting wear debris volume could grow as sliding continued. In comparison, the scratch-end pile-up material in wedge formation did not change along with continuous sliding, suggesting that only initially deformed material can be released as debris. Plowing wear led to little direct debris release but the ridges could be removed by subsequent sliding plastic deformation and wear debris release. By quantitatively analyzing the topography of the abraded area, we could first reveal the volume of deformed material and their wear mechanism could inform the likelihood of the deformed material release as NPs.

Image analysis of the topography of the abraded area can calculate volumes of pile-up or scratch features (Figure 4 A, B). Both scratch and pile-up volumes increased linearly with the load (R² > 0.94), following the Archard law,⁹⁶ notably, the pile-up volume was 2.8–4.6 and 3.7–8.4 times higher than the scratch volume, for virgin and UV-aged LDPE, respectively (Figure 4 C, D). The higher pile-up over scratch volume is likely due to (1) pile-up material partially covering the scratch area, leading to a lower measured scratch volume than the actual volume (Figure S13), and (2) the elastic relaxation of the scratch due to the viscoelasticity of LDPE.⁹⁷ This is further supported by the smaller scratch height profiles than the tip geometry (Figure S14). Previous microscale wear of PE by sand grain impacts revealed that the relaxation can occur within a few hours of the impact and the scratch volume can be reduced up to 90% during 4 weeks.⁹⁸ Nevertheless, this result implies that pile-up volume is a more reliable and relevant measure of NPs generation compared with scratch volume; thus, our following analysis focused on the pile-up volume.

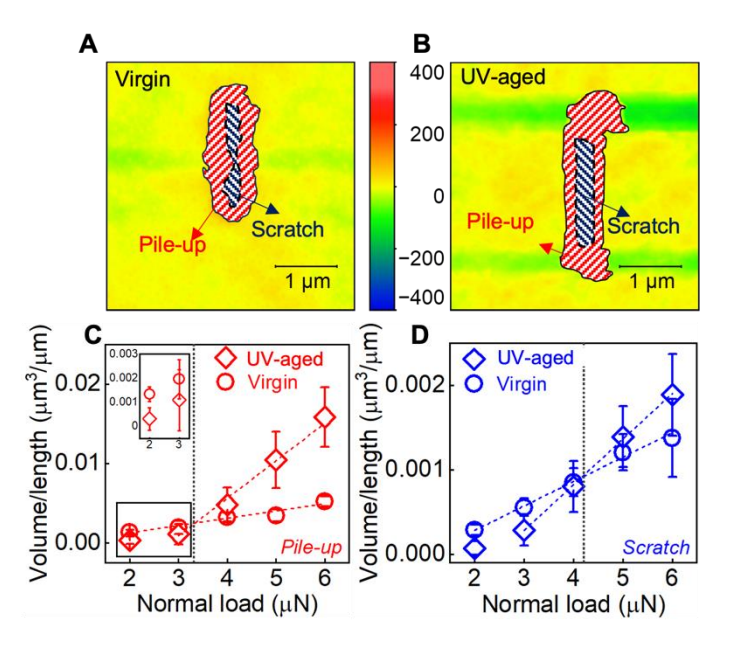


Figure 4. Nanoscale abrasive wear volume per sliding distance of UV-aged and virgin LDPE as an approximate of nanoplastic generation at the single asperity level. Representative topography images of **(A)** virgin and **(B)** UV-aged LDPE illustrate the raw topography data used for calculating pile-up and scratch volumes. The pile-up volume refers to the red strip highlighted area and the scratch volume refers to the blue strip highlighted area. The pile-up volume was always higher than the scratch volume for both LDPE samples. **(C)** Pile-up and **(D)** scratch volume per length of UV-aged LDPE are higher than that of virgin LDPE (note the difference in the scale of the two figures). However, the wear rate of LDPE was reduced after photoweathering at $2-3 \mu N$ (**inset**). Photoweathering does *not* always increase the wear rate of LDPE. The vertical dashed line indicates the load where the UV-aged LDPE started to have a higher wear than virgin LDPE. For each sample, there were 8-13 repeated wear volume data under each load.

Using pile-up volume data, the nanoscale abrasive wear coefficient of virgin LDPE, expressed in units of $\mu m^3/\mu m$ sliding distance/ μN normal load (slope of Figure 4C), was measured and calculated to be 1.0×10^{-3} at the single asperity level. Only data from 3–6 μN were used for calculating this slope because of the near-zero wear rate at 2 μN for UV-aged LDPE (discussed in the next section). This wear rate is lower than previously reported wear rates for PEs performed under macroscale wear (Figure S15), likely due to the difference in asperity size and load-dependent wear mechanism. ⁹⁹ In comparison, the wear coefficient of the UV-aged LDPE was 4.9 times higher (4.9 \times 10⁻³ μ m/ μ m/ μ N). Furthermore, the lateral signal and its slope with the load during the nanoscratch test was around 3-fold lower for UV-aged LDPE (Figure S16), implying that it required less energy transfer from frictional force to create abrasive wear for UV-aged LDPE compared with virgin ones. Furthermore, the potential NP release rate for UV-aged LDPE by the cutting mechanism is likely over 4.9 times higher than the rate for virgin LDPE by the plowing

mechanism (see last section). Our finding suggests that virgin ductile LDPE tends to plastically deform rather than release NPs via cutting wear. This implies that the current laboratory-scale MP/NPs preparation methods using mechanical milling of *virgin* plastics^{100, 101} may create particle properties distinct from environmental MP/NPs.

The impact of photooxidation on the overall abrasive wear rate of LDPE observed here was consistent with previous findings on MP release^{28, 102} and the understanding of the impact of polymer properties on wear rates. From the mechanics of materials perspective, the widely used Ratner-Lancaster correlation¹⁰³ predicts that the wear rate correlates with the reciprocal product of ultimate stress and the strain at break. The completely embrittled LDPE in this study had near zero stress and strain at break, supporting the higher wear coefficient. In the space of molecular and structural properties of semicrystalline polymers, some recent studies highlighted the important role of interlamellar phase properties including chain entanglement,⁹⁹ tie chain,^{104, 105} and interphase fraction¹⁰⁶, in reducing the propensity to wear. The entanglement of LDPE in this study was likely destroyed after two decades of MW reduction (Figure 1C), down to near entanglement molar mass for PE.¹⁰⁷ In addition, previous studies have evidenced interlamellar shrinking and the reduction of the tie chain in photooxidized PE.⁶⁵ Both evidence can support the increased wear rate of UV-aged LDPE.

Impact of Photooxidation on the Wear Rate of LDPE Is Load-Dependent.

Despite the overall trend of increasing wear rate due to photoweathering, unexpectedly, at $2-3~\mu N$, UV-aged LDPE had less visibly shallower scratches and less pile-up volume compared to virgin ones (Figure 3C). This can be further seen in the quantified wear rate (inset of Figure 4C, D). This resistance to wear is consistent with the observed higher load at the onset of wear for UV-aged LDPE observed during friction measurements (Figure 2A). Clearly, in this load regime, the wear rate and polymer properties correlation for UV-aged LDPE disobey the previous findings detailed above. We hypothesize that this is likely attributed to an increase in crystallinity (Figure 1D) as well as nanoindentation hardness and elastic modulus (Figure 5). Nanoindentation results analyzed using a properly selected contact mechanics model (JKR model) suggested that photoweathering increased the nanohardness and elastic modulus of LDPE by 10.7-fold and 9.3-fold, respectively. The increase in elastic modulus is consistent with previous tensile test results. At the interfacial region, it takes a higher load (or pressure) to initiate plastic deformation of UV-

aged LDPE which is opposed to the hardness. In addition, the tangential motion of sliding is opposed by wearless frictional force, which was also higher for UV-aged LDPE (Figure 2A). Both can be reflected as the coefficient of friction μ in the numerator and the hardness in the denominator of the RL correlation.¹⁰³ At a higher load (>4 μ N), the abrasive wear rate is correlated with stress and strain at break which was substantially declined for UV-aged LDPE. To the best of our knowledge, this is the first time such unexpected wear behavior was revealed for UV-aged LDPE at the nanoscale, suggesting that NPs release does not always increase for LDPE after photoweathering.

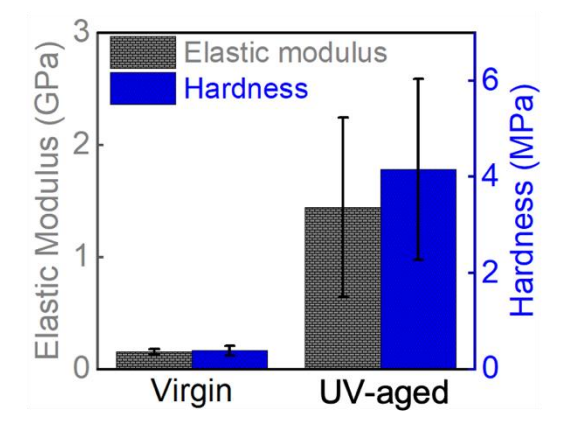


Figure 5. Increased hardness and elastic modulus of LDPE after photoweathering. Photoweathering caused the elastic modulus (left y-axis) to increase from 0.174 ± 0.027 GPa (virgin) to 1.627 ± 0.906 GPa (UV-aged). A similar trend was found for hardness (right y-axis), which was almost 11-fold higher for the UV-aged LDPE (4.67 ± 2.133 MPa) compared with the virgin LDPE (0.434 ± 0.113 MPa). The values were calculated by fitting the load and indentation depth using the JKR model, which was determined based on the adhesion-dependent transition parameter. Each force curve was collected with sufficient spacing (> 3 times the probe diameter) between two indentation locations.

New Parameter to Evaluate the Wear Mechanism for LDPE Implying NP Release.

Considering the complete process of NP release from nanoscale abrasive wear, the piled-up materials have to be released into free particles. While our method cannot directly observe this process, we hypothesize that the scratch end pile-up materials in the cutting wear case are highly likely loose enough to be released easily. Indeed, a previously developed concept by Kato and co–workers⁹⁰⁻⁹² developed a parameter named Degree of Wear to evaluate the propensity of releasing debris of given wear mechanisms. We adopted the concept to approximate the likelihood of pile-up material release as NPs. The Degree of Wear is defined as $\beta = \frac{A'-A''}{A'}$, where A' and A''

are the cross-sectional areas of the scratch (groove) and pile-up (ridge) at both sides of the scratch, respectively. As the scratch length is fixed, A' - A'' and A' correspond to the removable and total wear volume. Plowing has a $\beta \sim 0$, wedge formation has a $0 < \beta < 1$, and cutting wear has a $\beta \sim 1$. However, this formula cannot directly be used for our samples or viscoelastic materials in general, because (1) the scratch profile underestimates the total wear volume due to elastic relaxation of the scratch, and (2) the cross-sectional area along the scratch varied significantly along the sliding direction (Figures 3 and S17). We propose a new degree of wear $\beta' = \frac{v''}{v'}$ for viscoelastic materials, where V'' is the volume of pile-up at the scratch end (dotted area shown in Figure 6A, B) and V' is the total pile-up volume. Our proposal of directly using measured wear volume can be better suited to calculate the ratio of the removable wear volume and the total wear volume that Kato and coworkers⁹⁰ intended to describe. For virgin LDPE, β' ranged from 0.15 to 0.32 from the entire 2–6 μ N range. In comparison, the UV-aged LDPE had a β' of 0.41 and 0.53 for 2 and 3 μ N normal loads, respectively, and β' ranged from 0.85 to 0.9 for 4–6 μ N (Figure 6C). Based on our qualitative evaluation of the wear mechanism (Figure 4C, D), we propose regimes of β' to distinguish the wear mechanism: $0 < \beta' < 0.25$: plowing wear, $0.25 < \beta' < 0.75$: wedge formation, and $0.75 < \beta' < 1$: cutting wear. The new β' can be used to describe the abrasive wear mechanism of other viscoelastic materials at the nanoscale. Our method of investigating nanoscale abrasives enabled this new and reliable way of evaluating the degree of wear for plastics. By multiplying the new β' with the wear rate estimated using pile-up volume, we report $0.4 \times 10^{-3} \, \mu \text{m}^3 / \mu \text{m} / \mu \text{N}$ for virgin LDPE and 4.6×10⁻³ µm³/µm /µN for UV-aged LDPE. Considering this likelihood of release step, photoweathering may increase NP release by nanoscale abrasive wear by 10.6 times. We note that this is an initial estimation of NP release from the pile-up volume. We need future assessment of the characteristics of the pile-up materials and the true NP release rate needs careful validation by further work.

427

428

429

430

431

432

433

434

435

436

437

438

439

440

441

442

443

444

445

446

447

448

449

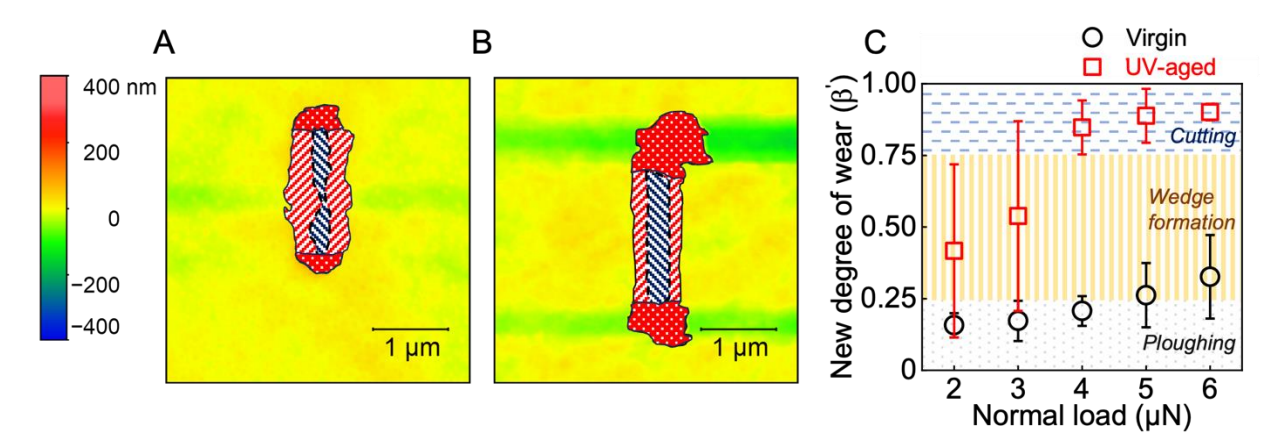


Figure 6: Proposed new Degree of Wear for elucidating the wear mechanism of viscoelastic materials. Representative topography images of **(A)** virgin and **(B)** UV-aged LDPE illustrate the raw topography data used for calculating pile-up volumes at the scratch end, where the red dotted area refers to the pile-up volume at the end. **(C)** β' quantitatively describes wear debris release via plowing, wedge formation, and cutting wear mechanisms. Note the large error bars of β' for 2 and 3 μ N were due to that the <25 nm pile-up features were difficult to differentiate from the surrounding roughness.

Environmental Implications

Our single asperity approach enabled by LFM elucidated new mechanistic insights into nanoscale abrasive wear that impacts NPs formation and potential release rates. This is a two-step process including (1) plastic deformation and (2) deformed material detachment into NPs. Our method enabled the exploration of nanoscale wear mechanisms (step 1) and can inform the second step of NP release. A lower rate of debris release for virgin LDPE is due to the plowing and wedge formation mechanism, compared with primarily cutting wear for UV-aged LDPE implying high debris release. We also report that UV-aged LDPE is unexpectedly resistant to wear compared with virgin LDPE under gentle abrasion conditions. This suggests that it is harder for slow-moving fine sediments to abrade UV-aged LDPE than virgin LDPE. Furthermore, using our precise topography measurement, we proposed a modified Degree of Wear as an initial approximation for estimating the likelihood of NP release from the pile-up (second step). Finally, using a 300 nm size tip, we found that nanoscale abrasive wear exclusively generates NPs less than 1 µm.

A major contribution of our approach is the ability to calculate a wear rate with a unit of mass of NPs/load/time for the nanoscale abrasive wear process, compared with previously reported NPs/time with no characterization of mechanical stress, ²⁸ or wear mass/load/distance. ^{42, 43} Such wear rate values will enable the conversion of laboratory-scale mechanical weathering study into

actual plastic degradation under realistic environmental conditions without the need to test it under every single environmental scenario. Assuming the pile-up volume can be released as 100 nm NPs, we estimate potential NP release rates of 0.3 and 3.3 NPs/μN/s per sliding, for virgin and UV-aged plastic, respectively, under the sliding velocity in this study. Considering velocities in creep aeolian transport (0–0.14 m/s), ⁸⁷ we expect up to 5 × 10⁴–1 × 10⁶ NPs/μN/s per sliding. NP release rate is 10 times higher after photoweathering of LDPE. This finding could be applied to other semicrystalline and rubbery polymer wastes (e.g., polypropylene), ¹⁰⁸ and our tools can be applied to other plastic waste. Future work is needed to validate the probability or fraction that the pile-up volume can be released as NPs and how it can be impacted by abrasion conditions. Our initial estimation lays a critical foundation for determining true NP release via the nanoscale abrasive wear process.

Our findings on the nanoscale abrasive wear process can best simulate the creep transport of sand grains (i.e., rolling and sliding) with nanosize asperities on plastic films at the top layer of sand or soil column and can be applied to fluvial and swash zones in future studies. Recent field observations reported unique "rock-plastic complex" and "plasticrust" in which plastic debris is integrated with inorganic rocks in river and shore environments, suggesting the environmental relevance and importance of sediment and plastic interactions. Creep is a major type of aeolian sand transport, 87, 88, 111 fluvial, 112 and swash zone 113 bedload movement. The NP release rate in aquatic sediment transport is likely higher due to a higher sediment transport velocity. 114 Additional work is needed given the differences in creep sand size, friction, and wear between air and water. In addition, nanoscale abrasive wear of UV-aged plastic under aquatic conditions could also promote the release of dissolved organic carbon along with solid NPs. Ultimately, such rates can be converted into the specific surface degradation rate 34 to calculate the lifetime of plastics, enabling life cycle assessment of polymers that incorporate the end-of-life impacts. 115

Finally, our findings reveal the difference in abrasive wear at the nanoscale compared with micro- and macroscales, which can lead to different implications regarding MP/NP release. In particular, the asperity size and load can impact the size of wear debris, rate, wear-polymer property correlations, and the role of photoweathering on wear. We highlight the need to study NP release by abrasive wear under *environmentally* relevant asperity size and applied load and to reveal the wear mechanism if possible. Further studies are needed to expand our findings that were

- limited to the 300 nm asperity and a velocity ~4 orders of magnitude lower than the sediment
- velocities in air.87

Supporting Information

- 509 Experimental details, AFM-IR results, replicates for the onset of wear and wear coefficient on
- 510 LDPE samples, topographic images collected simultaneously with friction map, topographic
- 511 images of LDPE samples, calculation of environmentally relevant forces, comparison of height
- 512 profile among LDPE samples and the probe, horizontal view of 3D scratch, correlation of wear
- 513 coefficient with crystallinity and molecular weight, lateral signal during nanoscratch experiment,
- 514 penetration depth under different normal loads.

515 **Author Information**

516 Corresponding Author

- 517 **Boya Xiong** Department of Civil, Environmental, and Geo-Engineering, University of
- 518 *Minnesota, 500 Pillsbury Dr SE, Minneapolis, MN 55455, United States.* Email: bxiong@umn.edu
- 519 Authors

532

- **Ehsanur Rahman** ‡ Department of Civil, Environmental, and Geo-Engineering, University of
- 521 *Minnesota, 500 Pillsbury Dr SE, Minneapolis, MN 55455, United States.*
- **Sara BinAhmed** ‡ Department of Civil, Environmental, and Geo-Engineering, University of
- 523 Minnesota, 500 Pillsbury Dr SE, Minneapolis, MN 55455, United States.
- **Phoebe Keyes** Department of Civil, Environmental, and Geo-Engineering, University of
- 525 Minnesota, 500 Pillsbury Dr SE, Minneapolis, MN 55455, United States.
- 526 Claire Alberg Department of Civil, Environmental, and Geo-Engineering, University of
- 527 *Minnesota*, 500 Pillsbury Dr SE, Minneapolis, MN 55455, United States.
- 528 **Stacy Godfreey-Igwe** Department of Mechanical Engineering, Massachusetts Institute of
- 529 Technology, 33 Massachusetts Ave, Cambridge, MA 02139, United States.
- 530 **Greg Haugstad** Characterization Facility, University of Minnesota, 100 Union St. SE,
- 531 Minneapolis, Minnesota 55455, United States.

533 ‡Both authors contributed equally to this work

Notes

The authors declare no competing financial interest.

Acknowledgments

This work was supported by the National Science Foundation Center for Sustainable Polymers headquartered at the University of Minnesota, Twin Cities, CHE-1901635. Parts of this work were carried out in the Characterization Facility, University of Minnesota, which receives partial support from the NSF through the MRSEC (Award Number DMR-2011401) and the NNCI (Award Number ECCS-2025124) programs. The cover artwork was created in collaboration with John Beumer at the NSF Center for Sustainable Polymers.

545 References

- 546 (1) Thompson, R. C.; Olsen, Y.; Mitchell, R. P.; Davis, A.; Rowland, S. J.; John, A. W. G.;
- McGonigle, D.; Russell, A. E. Lost at Sea: Where Is All the Plastic? Science 2004, 304 (5672),
- 548 838-838.
- 549 (2) Rochman, C. M.; Browne, M. A.; Halpern, B. S.; Hentschel, B. T.; Hoh, E.; Karapanagioti, H.
- 550 K.; Rios-Mendoza, L. M.; Takada, H.; Teh, S.; Thompson, R. C. Classify plastic waste as
- 551 hazardous. *Nature* **2013**, *494* (7436), 169–171.
- 552 (3) Bouwmeester, H.; Hollman, P. C. H.; Peters, R. J. B. Potential Health Impact of
- Environmentally Released Micro- and Nanoplastics in the Human Food Production Chain:
- Experiences from Nanotoxicology. *Environ. Sci. Technol.* **2015**, 49 (15), 8932–8947.
- 555 (4) Shi, Q.; Tang, J.; Wang, L.; Liu, R.; Giesy, J. P. Combined cytotoxicity of polystyrene
- 556 nanoplastics and phthalate esters on human lung epithelial A549 cells and its mechanism.
- *Ecotoxicology Environmental and Safety* **2021**, *213*, 112041.
- 558 (5) Schwabl, P.; Köppel, S.; Königshofer, P.; Bucsics, T.; Trauner, M.; Reiberger, T.; Liebmann,
- B. Detection of Various Microplastics in Human Stool. Annal of Internal Medicine 2019, 171,
- 560 453-457.
- 561 (6) Ji, Y.; Wang, C.; Wang, Y.; Fu, L.; Man, M.; Chen, L. Realistic polyethylene terephthalate
- nanoplastics and the size- and surface coating-dependent toxicological impacts on zebrafish
- 563 embryos. *Environmental Science: Nano* **2020**, *7*, 2313–2324.
- 564 (7) Kwak, J. I.; An, Y.-J. Microplastic digestion generates fragmented nanoplastics in soils and
- damages earthworm spermatogenesis and coelomocyte viability. *Journal of hazardous materials*
- **2021**, *402*, 124034.
- 567 (8) Lian, J.; Wu, J.; Xiong, H.; Zeb, A.; Yang, T.; Su, X.; Su, L.; Liu, W. Impact of polystyrene
- nanoplastics (PSNPs) on seed germination and seedling growth of wheat (Triticum aestivum L.).
- *Journal of Hazardous Materials* **2020**, *385*, 121620.
- 570 (9) Stubbins, A.; Law, K. L.; Muñoz, S. E.; Bianchi, T. S.; Zhu, L. Plastics in the Earth system.
- 571 *Science* **2021**, *373* (6550), 51–55.
- 572 (10) Revell, L. E.; Kuma, P.; Le Ru, E. C.; Somerville, W. R.; Gaw, S. Direct radiative effects of
- 573 airborne microplastics. *Nature* **2021**, *598* (7881), 462–467.
- 574 (11) Kvale, K.; Oschlies, A. Recovery from microplastic-induced marine deoxygenation may take
- 575 centuries. *Nature Geoscience* **2023**, *16* (1), 10–12.

- 576 (12) Ockelford, A.; Cundy, A.; Ebdon, J. E. Storm Response of Fluvial Sedimentary Microplastics.
- 577 *Sci. Rep.* **2020**, *10* (1), 1865.
- 578 (13) Gigault, J.; El Hadri, H.; Nguyen, B.; Grassl, B.; Rowenczyk, L.; Tufenkji, N.; Feng, S.;
- 579 Wiesner, M. Nanoplastics are neither microplastics nor engineered nanoparticles. *Nat.*
- 580 *Nanotechnol.* **2021**, *16* (5), 501–507.
- 581 (14) Mitrano, D. M.; Wick, P.; Nowack, B. Placing nanoplastics in the context of global plastic
- 582 pollution. *Nat. Nanotechnol.* **2021**, *16*, 491–500.
- 583 (15) CEFSA Panel on Contaminants in the Food Chain Presence of microplastics and nanoplastics
- in food, with particular focus on seafood. *EFSA J.* **2016**, *14* (6), e04501.
- 585 (16) Meides, N.; Menzel, T.; Poetzschner, B. r.; Löder, M. G.; Mansfeld, U.; Strohriegl, P.;
- Altstaedt, V.; Senker, J. r. Reconstructing the environmental degradation of polystyrene by
- 587 accelerated weathering. *Environ. Sci. Technol.* **2021**, *55* (12), 7930–7938.
- 588 (17) Hernandez, L. M.; Grant, J.; Fard, P. S.; Farner, J. M.; Tufenkji, N. Analysis of ultraviolet
- and thermal degradations of four common microplastics and evidence of nanoparticle release.
- *Journal of Hazardous Materials Letters* **2023**, *4*, 100078.
- 591 (18) Enfrin, M.; Lee, J.; Gibert, Y.; Basheer, F.; Kong, L.; Dumée, L. F. Release of hazardous
- 592 nanoplastic contaminants due to microplastics fragmentation under shear stress forces. *Journal of*
- 593 *hazardous materials* **2020**, *384*, 121393.
- 594 (19) Pfohl, P.; Wagner, M.; Meyer, L.; Domercq, P.; Praetorius, A.; Hüffer, T.; Hofmann, T.;
- Wohlleben, W. Environmental degradation of microplastics: how to measure fragmentation rates
- to secondary micro-and nanoplastic fragments and dissociation into dissolved organics. *Environ*.
- 597 Sci. Technol. **2022**, 56 (16), 11323–11334.
- 598 (20) Yang, T.; Luo, J.; Nowack, B. Characterization of nanoplastics, fibrils, and microplastics
- released during washing and abrasion of polyester textiles. *Environ. Sci. Technol.* **2021**, *55* (23),
- 600 15873-15881.
- 601 (21) Mattsson, K.; Björkroth, F.; Karlsson, T.; Hassellöv, M. Nanofragmentation of Expanded
- 602 Polystyrene Under Simulated Environmental Weathering (Thermooxidative Degradation and
- Hydrodynamic Turbulence). Frontiers in Marine Science 2021, 7, 578178.
- 604 (22) Hernandez, L. M.; Xu, E. G.; Larsson, H. C. E.; Tahara, R.; Maisuria, V. B.; Tufenkji, N.
- Plastic Teabags Release Billions of Microparticles and Nanoparticles into Tea. Environ. Sci.
- 606 *Technol.* **2019**, *53*, 12300–12310.

- 607 (23) Su, Y.; Hu, X.; Tang, H.; Lu, K.; Li, H.; Liu, S.; Xing, B.; Ji, R. Steam disinfection releases
- 608 micro (nano) plastics from silicone-rubber baby teats as examined by optical photothermal infrared
- 609 microspectroscopy. *Nat. Nanotechnol.* **2022**, *17* (1), 76–85.
- 610 (24) Hadiuzzaman, M.; Salehi, M.; Fujiwara, T. Plastic litter fate and contaminant transport within
- the urban environment, photodegradation, fragmentation, and heavy metal uptake from storm
- 612 runoff. *Environmental Research* **2022**, *212*, 113183.
- 613 (25) Dawson, A. L.; Kawaguchi, S.; King, C. K.; Townsend, K. A.; King, R.; Huston, W. M.;
- Nash, S. M. B. Turning microplastics into nanoplastics through digestive fragmentation by
- 615 Antarctic krill. *Nat. Commun.* **2018**, 9 (1), 1001.
- 616 (26) Battacharjee, L.; Jazaei, F.; Salehi, M. Insights into the mechanism of plastics' fragmentation
- under abrasive mechanical forces: An implication for agricultural soil health. Clean: Soil, Air,
- 618 *Water* **2023**, *51* (8), 2200395.
- 619 (27) Ward, C. P.; Armstrong, C. J.; Walsh, A. N.; Jackson, J. H.; Reddy, C. M. Sunlight converts
- 620 polystyrene to carbon dioxide and dissolved organic carbon. Environmental Science & Technology
- 621 Letters **2019**, 6 (11), 669–674.
- 622 (28) Song, Y. K.; Hong, S. H.; Jang, M.; Han, G. M.; Jung, S. W.; Shim, W. J. Combined effects
- of UV exposure duration and mechanical abrasion on microplastic fragmentation by polymer type.
- 624 Environ. Sci. Technol. **2017**, 51 (8), 4368–4376.
- 625 (29) Chubarenko, I.; Efimova, I.; Bagaeva, M.; Bagaev, A.; Isachenko, I. On mechanical
- 626 fragmentation of single-use plastics in the sea swash zone with different types of bottom
- sediments: Insights from laboratory experiments. *Marine pollution bulletin* **2020**, *150*, 110726.
- 628 (30) Bossa, N.; Sipe, J. M.; Berger, W.; Scott, K.; Kennedy, A.; Thomas, T.; Hendren, C. O.;
- Wiesner, M. R. Quantifying Mechanical Abrasion of MWCNT Nanocomposites used in 3D
- Printing: Influence of CNT content on abrasion products and rate of microplastic production.
- 631 Environ. Sci. Technol. **2021**, 55 (15), 10332–10342.
- 632 (31) Hebner, T. S.; Maurer-Jones, M. A. Characterizing microplastic size and morphology of
- photodegraded polymers placed in simulated moving water conditions. *Environmental Science*:
- 634 *Processes & Impacts* **2020**, *22* (2), 398–407.
- 635 (32) Cui, Q.; Yang, X.; Li, J.; Miao, Y.; Zhang, X. Microplastics Generation Behavior of
- Polypropylene Films with Different Crystalline Structures under UV Irradiation. *Polym. Degrad.*
- 637 Stab. 2022, 109916.

- 638 (33) Ter Halle, A.; Ladirat, L.; Gendre, X.; Goudouneche, D.; Pusineri, C.; Routaboul, C.;
- 639 Tenailleau, C.; Duployer, B.; Perez, E. Understanding the fragmentation pattern of marine plastic
- debris. Environ. Sci. Technol. **2016**, 50 (11), 5668–5675.
- 641 (34) Chamas, A.; Moon, H.; Zheng, J.; Qiu, Y.; Tabassum, T.; Jang, J. H.; Abu-Omar, M.; Scott,
- S. L.; Suh, S. Degradation Rates of Plastics in the Environment. ACS Sustainable Chem. Eng.
- **2020**, 8 (9), 3494–3511.
- 644 (35) Burwell Jr, J. T. Survey of possible wear mechanisms. *Wear* **1957**, *1* (2), 119–141.
- 645 (36) Lancaster, J. K. Material-specific wear mechanisms: relevance to wear modelling. *Wear* **1990**,
- 646 *141* (1), 159-183.
- 647 (37) Lancaster, J. Abrasive wear of polymers. *Wear* **1969**, *14* (4), 223–239.
- 648 (38) Sun, Z.; Mehmani, A.; Torres-Verdín, C. Subpore-Scale Trapping Mechanisms Following
- Imbibition: A Microfluidics Investigation of Surface Roughness Effects. *Water Resour. Res.* **2021**,
- 650 57 (2), e2020WR028324, https://doi.org/10.1029/2020WR028324.
- 651 (39) Bousbaa, C.; Madjoubi, M.; Hamidouche, Z.; Bouaouadja, N. Effect Of Sand Blasting On
- 652 Soda Lime Glass Properties. *Eng. J. Univ. Qatar* **2003**, *16*, 125–138.
- 653 (40) Ashby, M. F. Chapter 4 Material Property Charts. In Materials Selection in Mechanical
- 654 Design (Fourth ed.); Ashby, M. F., Ed.; Butterworth-Heinemann: 2011; pp 57–96.
- 655 (41) Bullard, J. E.; Zhou, Z.; Davis, S.; Fowler, S. Breakdown and modification of microplastic
- beads by aeolian abrasion. *Environ. Sci. Technol.* **2023**, *57* (1), 76–84.
- 657 (42) Yoon, E.-S.; Singh, R. A.; Oh, H.-J.; Kong, H. The effect of contact area on nano/micro-scale
- 658 friction. Wear **2005**, 259 (7–12), 1424–1431.
- 659 (43) Omar, M. K.; Atkins, A. G.; Lancaster, J. K. The role of crack resistance parameters in
- 660 polymer wear. J. Phys. D: Appl. Phys. **1986**, 19 (2), 177.
- 661 (44) Shipway, P.; Ngao, N. Microscale abrasive wear of polymeric materials. Wear 2003, 255
- 662 (1-6), 742-750.
- 663 (45) Bhushan, B. Nanotribology, Nanomechanics and Materials Characterization. In *Springer*
- 664 *Handbook of Nanotechnology*; Bhushan, B., Ed.; Springer: Berlin Heidelberg, 2017; pp 869–934.
- 665 (46) Tambe, N. S.; Bhushan, B. Nanoscale friction and wear maps. *Philos. Trans. R. Soc., A* 2008,
- 666 *366* (1869), 1405–1424.
- 667 (47) Haugstad, G. Atomic force microscopy: understanding basic modes and advanced
- applications; John Wiley & Sons: 2012.

- 669 (48) Celano, U.; Hsia, F.-C.; Vanhaeren, D.; Paredis, K.; Nordling, T. E.; Buijnsters, J. G.;
- Hantschel, T.; Vandervorst, W. Mesoscopic physical removal of material using sliding nano-
- 671 diamond contacts. Sci. Rep. **2018**, 8 (1), 2994.
- 672 (49) Walker, J.; Umer, J.; Mohammadpour, M.; Theodossiades, S.; Bewsher, S. R.; Offner, G.;
- Bansal, H.; Leighton, M.; Braunstingl, M.; Flesch, H.-G. Asperity level characterization of
- abrasive wear using atomic force microscopy. *Proc. R. Soc. A* **2021**, 477 (2250), 20210103.
- 675 (50) Furustig, J.; Dobryden, I.; Almqvist, A.; Almqvist, N.; Larsson, R. The measurement of wear
- using AFM and wear interpretation using a contact mechanics coupled wear model. Wear 2016,
- 677 *350–351*, 74–81.
- 678 (51) Tambe, N. S.; Bhushan, B. Nanoscale friction-induced phase transformation of diamond-like
- 679 carbon. *Scripta Materialia* **2005**, *52* (8), 751–755.
- 680 (52) Fang, T.-H.; Chang, W.-J.; Tsai, S.-L. Nanomechanical characterization of polymer using
- atomic force microscopy and nanoindentation. *Microelectronics Journal* **2005**, *36* (1), 55–59.
- 682 (53) Fayolle, B.; Colin, X.; Audouin, L.; Verdu, J. Mechanism of degradation induced
- 683 embrittlement in polyethylene. *Polym. Degrad. Stab.* **2007**, *92* (2), 231–238.
- 684 (54) Liu, L.; Duan, H.; Zhan, W.; Zhan, S.; Jia, D.; Li, Y.; Li, C.; An, J.; Du, C.; Li, J. Effects of
- 685 UV irradiation time on the molecular structure of typical engineering plastics and tribological
- 686 properties under heavy load. *High Perform. Polym.* **2022**, *34* (3), 352–362.
- 687 (55) Choudhury, M.; Hutchings, I. The effects of irradiation and ageing on the abrasive wear
- resistance of ultra high molecular weight polyethylene. Wear 1997, 203, 335–340.
- 689 (56) Alshibli Khalid, A.; Alsaleh M. I. Characterizing Surface Roughness and Shape of Sands
- 690 Using Digital Microscopy. *J. Comput. Civil Eng.* **2004**, *18* (1), 36–45.
- 691 (57) Rasmuson, A.; Pazmino, E.; Assemi, S.; Johnson, W. P. Contribution of nano-to microscale
- roughness to heterogeneity: Closing the gap between unfavorable and favorable colloid attachment
- 693 conditions. *Environ. Sci. Technol.* **2017**, *51* (4), 2151–2160.
- 694 (58) Altuhafi F.; Coop M. R.; Georgiannou V. N. Effect of Particle Shape on the Mechanical
- 695 Behavior of Natural Sands. J. Geotech. Geoenviron. Eng. **2016**, 142 (12), 04016071.
- 696 (59) Yang, H.; Baudet, B. A.; Yao, T. Characterization of the surface roughness of sand particles
- 697 using an advanced fractal approach. Proceedings of the Royal Society A: Mathematical, Physical
- 698 and Engineering Sciences **2016**, 472 (2194), 20160524.

- 699 (60) Hutter, J. L.; Bechhoefer, J. Calibration of atomic-force microscope tips. *Review of scientific*
- 700 instruments **1993**, 64 (7), 1868–1873.
- 701 (61) Tang, B.; Ngan, A.; Pethica, J. A method to quantitatively measure the elastic modulus of
- materials in nanometer scale using atomic force microscopy. Nanotechnology 2008, 19 (49),
- 703 495713.
- 704 (62) Briscoe, B.; Fiori, L.; Pelillo, E. Nano-indentation of polymeric surfaces. J. Phys. D: Appl.
- 705 *Phys.* **1998**, *31* (19), 2395.
- 706 (63) Dokukin, M. E.; Sokolov, I. On the measurements of rigidity modulus of soft materials in
- nanoindentation experiments at small depth. *Macromolecules* **2012**, *45* (10), 4277–4288.
- 708 (64) Hsueh, H.-C.; Kim, J. H.; Orski, S.; Fairbrother, A.; Jacobs, D.; Perry, L.; Hunston, D.; White,
- 709 C.; Sung, L. Micro and macroscopic mechanical behaviors of high-density polyethylene under UV
- irradiation and temperature. *Polym. Degrad. Stab.* **2020**, *174*, 109098.
- 711 (65) Hsu, Y.-C.; Weir, M. P.; Truss, R. W.; Garvey, C. J.; Nicholson, T. M.; Halley, P. J. A
- fundamental study on photo-oxidative degradation of linear low density polyethylene films at
- 713 embrittlement. *Polymer* **2012**, *53* (12), 2385–2393.
- 714 (66) Ranjan, V. P.; Goel, S. Degradation of low-density polyethylene film exposed to UV radiation
- in four environments. J. Hazard., Toxic, Radioact. Waste 2019, 23 (4), 04019015.
- 716 (67) Syranidou, E.; Karkanorachaki, K.; Barouta, D.; Papadaki, E.; Moschovas, D.; Avgeropoulos,
- 717 A.; Kalogerakis, N. Relationship between the Carbonyl Index (CI) and Fragmentation of
- Polyolefin Plastics during Aging. Environ. Sci. Technol. 2023, 57 (21), 8130–8138.
- 719 (68) Gulmine, J.; Janissek, P.; Heise, H.; Akcelrud, L. Degradation profile of polyethylene after
- artificial accelerated weathering. *Polym. Degrad. Stab.* **2003**, 79 (3), 385–397.
- 721 (69) Mundhenke, T. F.; Li, S. C.; Maurer-Jones, M. A. Photodegradation of polyolefin thin films
- in simulated freshwater conditions. *Environmental Science: Processes & Impacts* **2022**, *24* (12),
- 723 2284–2293.
- 724 (70) Grause, G.; Chien, M.-F.; Inoue, C. Changes during the weathering of polyolefins. *Polym.*
- 725 Degrad. Stab. **2020**, 181, 109364.
- 726 (71) Julienne, F.; Lagarde, F.; Delorme, N. Influence of the crystalline structure on the
- fragmentation of weathered polyolefines. *Polym. Degrad. Stab.* **2019**, *170*, 109012.
- 728 (72) Garnai Hirsch, S.; Barel, B.; Segal, E. Characterization of surface phenomena: probing early
- stage degradation of low-density polyethylene films. *Polym. Eng. Sci.* **2019**, *59* (S1), E129–E137.

- 730 (73) Suresh, B.; Maruthamuthu, S.; Kannan, M.; Chandramohan, A. Mechanical and surface
- properties of low-density polyethylene film modified by photo-oxidation. *Polym. J.* **2011**, *43* (4),
- 732 398–406.
- 733 (74) Atkinson, C.; Richardson, M. Thermodynamic properties of ideally crystalline polyethylene.
- 734 *Trans. Faraday Soc.* **1969**, *65*, 1764–1773.
- 735 (75) Niederberger, S.; Gracias, D.; Komvopoulos, K.; Somorjai, G. Transitions from nanoscale to
- microscale dynamic friction mechanisms on polyethylene and silicon surfaces. *Journal of applied*
- 737 *physics* **2000**, 87 (6), 3143–3150.
- 738 (76) Cho, D.-H.; Bhushan, B. Nanofriction and nanowear of polypropylene, polyethylene
- terephthalate, and high-density polyethylene during sliding. Wear 2016, 352-353, 18–23.
- 740 (77) Bahadur, S.; Ludema, K. C. The viscoelastic nature of the sliding friction of polyethylene,
- 741 polypropylene and copolymers. *Wear* **1971**, *18* (2), 109–128.
- 742 (78) Karuppiah, K. K.; Bruck, A. L.; Sundararajan, S.; Wang, J.; Lin, Z.; Xu, Z.-H.; Li, X. Friction
- and wear behavior of ultra-high molecular weight polyethylene as a function of polymer
- 744 crystallinity. *Acta Biomater.* **2008**, *4* (5), 1401–1410.
- 745 (79) Hammerschmidt, J. A.; Gladfelter, W. L.; Haugstad, G. Probing polymer viscoelastic
- relaxations with temperature-controlled friction force microscopy. *Macromolecules* **1999**, *32* (10),
- 747 3360-3367.
- 748 (80) Noy, A.; Frisbie, C. D.; Rozsnyai, L. F.; Wrighton, M. S.; Lieber, C. M. Chemical force
- microscopy: exploiting chemically-modified tips to quantify adhesion, friction, and functional
- 750 group distributions in molecular assemblies. J. Am. Chem. Soc. 1995, 117 (30), 7943–7951.
- 751 (81) Fuller, K.; Tabor, D. The effect of surface roughness on the adhesion of elastic solids. *Proc.*
- 752 R. Soc. London, Ser. A 1975, 345 (1642), 327–342.
- 753 (82) Archard, J. Elastic deformation and the laws of friction. *Proc. R. Soc. London, Ser. A* 1957,
- 754 *243* (1233), 190–205.
- 755 (83) Haugstad, G.; Gladfelter, W. L.; Weberg, E. B.; Weberg, R. T.; Jones, R. R. Probing molecular
- relaxation on polymer surfaces with friction force microscopy. *Langmuir* **1995**, *11* (9), 3473–3482.
- 757 (84) Xiong, J.; Ni, K.; Liao, X.; Zhu, J.; An, Z.; Yang, Q.; Huang, Y.; Li, G. Investigation of
- 758 chemi-crystallization and free volume changes of high-density polyethylene weathered in a
- 759 subtropical humid zone. *Polym. Int.* **2016**, *65* (12), 1474–1481.

- 760 (85) Sørensen, L.; Groven, A. S.; Hovsbakken, I. A.; Del Puerto, O.; Krause, D. F.; Sarno, A.;
- 761 Booth, A. M. UV degradation of natural and synthetic microfibers causes fragmentation and
- release of polymer degradation products and chemical additives. Sci. Total Environ. 2021, 755
- 763 143170.
- 764 (86) Liu, Z.; Zhu, Y.; Lv, S.; Shi, Y.; Dong, S.; Yan, D.; Zhu, X.; Peng, R.; Keller, A. A.; Huang,
- Y. Quantifying the Dynamics of Polystyrene Microplastics UV-Aging Process. *Environmental*
- 766 Science & Technology Letters **2022**, 9 (1), 50–56.
- 767 (87) Hong, C.; Xueyong, Z.; Chenchen, L.; Jiajia, H.; Yongqiu, W. Transport mass of creeping
- sand grains and their movement velocities. *Journal of Geophysical Research: Atmospheres* **2013**,
- 769 *118* (12), 6374–6382.
- 770 (88) Wang, Y.; Wang, D.; Wang, L.; Zhang, Y. Measurement of sand creep on a flat sand bed
- using a high-speed digital camera. Sedimentology 2009, 56 (6), 1705–1712.
- 772 (89) Aghababaei, R.; Warner, D. H.; Molinari, J.-F. Critical length scale controls adhesive wear
- 773 mechanisms. *Nat. Commun.* **2016**, 7 (1), 1–8.
- 774 (90) Kayaba, T.; Hokkirigawa, K.; Kato, K. Analysis of the abrasive wear mechanism by
- successive observations of wear processes in a scanning electron microscope. Wear 1986, 110 (3),
- 776 419–430.
- 777 (91) Kato, K. Micro-mechanisms of wear—wear modes. *Wear* **1992**, *153* (1), 277–295.
- 778 (92) Hokkirigawa, K.; Kato, K. An experimental and theoretical investigation of ploughing, cutting
- and wedge formation during abrasive wear. *Tribol. Int.* **1988**, *21* (1), 51–57.
- 780 (93) Soni, A.; Das, P. K.; Yusuf, M.; Ridha, S.; Kamyab, H.; Alam, M. A.; Masood, F.; Chelliapan,
- 781 S.; Ubaidullah, M.; Pandit, B.; et al. Synergy of silica sand and waste plastics as thermoplastic
- 782 composites on abrasive wear characteristics under conditions of different loads and sliding speeds.
- 783 *Chemosphere* **2023**, *323*, 138233.
- 784 (94) Alam, K. I.; Baratz, A.; Burris, D. Leveraging trace nanofillers to engineer ultra-low wear
- 785 polymer surfaces. *Wear* **2021**, *482*, 203965.
- 786 (95) Hutchings, I. M. Ductile-brittle transitions and wear maps for the erosion and abrasion of
- 787 brittle materials. *J. Phys. D: Appl. Phys.* **1992**, *25* (1A), A212.
- 788 (96) Archard, J. Contact and rubbing of flat surfaces. *Journal of applied physics* **1953**, 24 (8),
- 789 981–988.

- 790 (97) Hadal, R. S.; Misra, R. D. K. Scratch deformation behavior of thermoplastic materials with
- significant differences in ductility. *Materials Science and Engineering: A* **2005**, *398* (1), 252-261.
- 792 (98) Walley, S.; Field, J. E. The erosion and deformation of polyethylene by solid-particle impact.
- 793 *Philos. Trans. R. Soc. London; Ser A* **1987**, *321* (1558), 277–303.
- 794 (99) Tervoort, T. A.; Visjager, J.; Smith, P. On abrasive wear of polyethylene. *Macromolecules*
- **2002**, *35* (22), 8467–8471.
- 796 (100) McColley, C. J.; Nason, J. A.; Harper, B. J.; Harper, S. L. An assessment of methods used
- 797 for the generation and characterization of cryomilled polystyrene micro- and nanoplastic particles.
- 798 *Microplast. Nanoplast.* **2023**, *3* (1), 20.
- 799 (101) Smith, C.; Brown, S.; Malone, N.; Bevers, S.; Ranville, J.; Fairbrother, D. H. Nanoplastics
- prepared with uniformly distributed metal-tags: a novel approach to quantify size distribution and
- particle number concentration of polydisperse nanoplastics by single particle ICP-MS.
- 802 Environmental Science: Nano **2024**, 11, 911–923.
- 803 (102) Sun, J.; Zheng, H.; Xiang, H.; Fan, J.; Jiang, H. The surface degradation and release of
- microplastics from plastic films studied by UV radiation and mechanical abrasion. Science of The
- 805 *Total Environment* **2022**, 156369.
- 806 (103) Lancaster, J. K. Relationships between the Wear of Polymers and their Mechanical
- Properties. Proceedings of the Institution of Mechanical Engineers, Conference Proceedings 1968,
- 808 183 (16), 98–106.
- 809 (104) Ferreira, E. H.; Fechine, G. J. High abrasive wear resistance polyethylene blends: an adapted
- Ratner–Lancaster correlation. *Polym. Bull.* **2022**, 79, 3631–3648.
- 811 (105) Klapperich, C.; Komvopoulos, K.; Pruitt, L. Tribological properties and microstructure
- evolution of ultra-high molecular weight polyethylene. Journal of Tribology 1999, 121 (2),
- 813 394–402.
- 814 (106) Zhang, H.; Zhao, S.; Xin, Z.; Ye, C.; Li, Z.; Xia, J. Wear Resistance Mechanism of
- 815 Ultrahigh-Molecular-Weight Polyethylene Determined from Its Structure—Property Relationships.
- 816 *Ind. Eng. Chem. Res.* **2019**, *58* (42), 19519–19530.
- 817 (107) Raju, V. R.; Rachapudy, H.; Graessley, W. W. Properties of amorphous and crystallizable
- 818 hydrocarbon polymers. IV. Melt rheology of linear and star-branched hydrogenated
- 819 polybutadiene. J. Polym. Sci., Polym. Phys. Ed. 1979, 17 (7), 1223–1235.

- 820 (108) Fayolle, B.; Richaud, E.; Colin, X.; Verdu, J. degradation-induced embrittlement in semi-
- crystalline polymers having their amorphous phase in rubbery state. J. Mat. Sci. 2008, 43 (22),
- 822 6999-7012.
- 823 (109) Wang, L.; Bank, M. S.; Rinklebe, J.; Hou, D. Plastic-Rock Complexes as Hotspots for
- 824 Microplastic Generation. *Environ. Sci. Technol.* **2023**, *57* (17), 7009–7017.
- 825 (110) Gestoso, I.; Cacabelos, E.; Ramalhosa, P.; Canning-Clode, J. Plasticrusts: A new potential
- threat in the Anthropocene's rocky shores. *Science of The Total Environment* **2019**, 687, 413–415.
- 827 (111) Nickling, W. The initiation of particle movement by wind. Sedimentology 1988, 35 (3),
- 828 499-511.
- 829 (112) Kramer, H. Sand mixtures and sand movement in fluvial model. Transactions of the
- 830 *American Society of Civil Engineers* **1935**, *100* (1), 798–838.
- 831 (113) Horn, D. P.; Mason, T. Swash zone sediment transport modes. *Marine Geology* **1994**, *120*
- 832 (3), 309–325.

- 833 (114) Hughes, M. G.; Masselink, G.; Brander, R. W. Flow velocity and sediment transport in the
- swash zone of a steep beach. *Marine Geology* **1997**, *138* (1–2), 91–103.
- 835 (115) Maga, D.; Galafton, C.; Blömer, J.; Thonemann, N.; Özdamar, A.; Bertling, J. Methodology
- to address potential impacts of plastic emissions in life cycle assessment. *International Journal of*
- 837 *Life Cycle Assessment* **2022**, *27* (3), 469–491.